NANOSYSTEMS:
PHYSICS, CHEMISTRY, MATHEMATICS

Original article

Borisov V.A., et al. *Nanosystems: Phys. Chem. Math.*, 2025, **16** (4), 498–509.
http://nanojournal.ifmo.ru
DOI 10.17586/2220-8054-2025-16-4-498-509

La and Co-based materials for ammonia decomposition: activity, stability and structural changes

Vadim A. Borisov[1,a], Zaliya A. Fedorova[2,b], Zakhar N. Ichetovkin[3,4,c], Evgeniy Y. Gerasimov[2,d], Dmitry A. Shlyapin[2,e], Anna Y. Stroeva[3,f], Victor L. Temerev[1,g], Alexey B. Arbuzov[1,h], Sergey V. Tsybulya[2,j], Pavel V. Snytnikov[2,k], Anton V. Kuzmin[3,l]

[1]Center of New Chemical Technologies BIC, Boreskov Institute of Catalysis, Neftezavodskaya st., 54, Omsk, 644040, Russia

[2]Boreskov Institute of Catalysis, Lavrentiev Ave., 5, Novosibirsk, 630090, Russia

[3]Department of Technology of Inorganic Materials and Electrochemical Production, Vyatka State University, Moskovskaya st., 36, Kirov, 610000, Russia

[4]Institute of Solid State Chemistry and Mechanochemistry of the Siberian Branch of the RAS, Kutateladze st., 18, Novosibirsk, 630128, Russia

[a]borisovtiger86@mail.ru, [b]sabirova@catalysis.ru, [c]zakhar1030@mail.ru, [d]gerasimov@catalysis.ru, [e]dmitryshlyapin@yandex.ru, [f]stroevaanna@yandex.ru, [g]tvl@ihcp.ru, [h]arbuzov@ihcp.ru, [j]tsybulya@catalysis.ru, [k]pvsnyt@catalysis.ru, [l]a.v.kuzmin@yandex.ru

Corresponding author: V. A. Borisov, borisovtiger86@mail.ru

ABSTRACT The $La_{0.9}Sr_{0.1}Sc_{0.9}Co_{0.1}O_{3-\delta}$ (LS) and $La_{0.9}Sr_{0.1}CoO_{3-\delta}$ (LC) phases and composite materials based on them were synthesized. There are data in the literature on the activity of pure or modified forms of LC in ammonia decomposition, but there are no data on the activity of the LS phase and LS–LC composites. Therefore, the stability and activity of LS–LC composites and initial LS and LC in ammonia decomposition were investigated. The best result in the decomposition of ammonia at 700 °C and WHSV of 60000 ml $NH_3 \cdot g_{cat}^{-1} \cdot h^{-1}$ shows LC – 99%, the worst LS – 80%. Under the same conditions, the activity of samples LC, 40LS–60LC and 50LS–50LC remains unchanged for 40 hours. It was found that during ammonia decomposition, the LC phase decomposes to form cobalt and $La(OH)_3$ nanoparticles, but the LS phase does not undergo significant changes, which is confirmed by X-ray diffraction, IR spectroscopy, Raman spectroscopy and TEM.

KEYWORDS Ammonia decomposition, cobalt, lanthanum scandate, electrode materials.

ACKNOWLEDGEMENTS This work was supported by the Ministry of Science and Higher Education of the Russian Federation within the governmental assignment for the Boreskov Institute of Catalysis (project FWUR-2024-0039 and FWUR-2024-0033). Physico-chemical studies were carried out using facilities of the shared research center “National center of investigation of catalysts” at Boreskov Institute of Catalysis.

FOR CITATION Borisov V.A., Fedorova Z.A., Ichetovkin Z.N., Gerasimov E.Y., Shlyapin D.A., Stroeva A.Y., Temerev V.L., Arbuzov A.B., Tsybulya S.V., Snytnikov P.V., Kuzmin A.V. La and Co-based materials for ammonia decomposition: activity, stability and structural changes. *Nanosystems: Phys. Chem. Math.*, 2025, **16** (4), 498–509.

1. Introduction

It is believed that hydrogen energy technologies will prevent global warming and environmental pollution [1–4]. However, there are several key problems for the widespread introduction of hydrogen energy technologies: the explosiveness and low volumetric energy density of hydrogen, the complexity of its liquefaction, storage and transportation. Therefore, the problem of the hydrogen producing directly at the places of its consumption is relevant. On the other hand, ammonia is an excellent carrier of H_2 with a high hydrogen content (17.7 wt. %) and energy density (3000 W·h/kg), the ability to easy liquefaction at 0.8 MPa and 298 K, and wide availability (world NH_3 production is about 200 million tons, there are well-established ammonia market and logistics) [5–7].

Despite the high activity of ruthenium-containing ammonia decomposition catalysts [8–15], special attention has been paid to cobalt-containing systems [16–22]. One of the promising materials for use in solid oxide fuel cells (SOFCs), which are active in the process of ammonia decomposition, is lanthanum cobaltite $La_{0.9}Sr_{0.1}CoO_{3-\delta}$. In a hydrogen-containing environment, lanthanum cobaltite forms the phases Co and $LaCoO_x$, which are active in the decomposition of ammonia. Lanthanum cobaltite is also a promising electrode material. Typically, $LaCoO_x$ catalysts are widely used during the oxidation of CO and hydrocarbons [23–32]. Hu et al. showed that the La introduction promotes dissociative

adsorption of NH_3 and N_2 desorption, increasing the efficiency of ammonia decomposition [33]. Full ammonia cracking at weight hourly space velocity (WHSV) 30 000 $g_{cat}^{-1}\cdot h^{-1}$ and 550 °C was achieved on $LaCoO_x$/Co@NC/SBA-15 catalyst [20]. The excellent activity of the catalyst is combined with its high stability at high temperatures: the yield was 446 mmol $H_2\cdot gCo^{-1}\cdot min^{-1}$ at 600 °C and WHSV 60 000 $g_{cat}^{-1}\cdot h^{-1}$ during the 200 hour test. Amorphous $LaCoO_x$ particles significantly enhance NH_3 adsorption, while electron-rich Co^0 particles promote NH_3 activation and associative desorption of surface-bound N atoms. In combination with other lanthanides and alkali metals, cobalt catalysts also exhibit high activity [22].

It is possible to combine the decomposition of ammonia and the conversion of the resulting hydrogen within the framework of a single device – proton-ceramic fuel cell (PCFC) with a two-layer anode performing a dual function: catalytic decomposition of ammonia into nitrogen and hydrogen and electrocatalytic oxidation of hydrogen [34, 35]. One of the most suitable compounds is lanthanum scandate–based materials, among which $La_{0.9}Sr_{0.1}ScO_{3-\delta}$ has the highest conductivity. Similar electrode materials have been proposed for this electrolyte, one of which is $La_{0.9}Sr_{0.1}Sc_{0.9}Co_{0.1}O_{3-\delta}$ [36], which is well compatible with $La_{0.9}Sr_{0.1}ScO_{3-\delta}$ and lanthanum cobaltites.

Currently, there are many articles devoted to PCFC based on ammonia fuels, which demonstrate a wide power range from 0.03 to 1 $W\cdot cm^{-2}$ in the operating temperature range of 600–700 °C [37]. The level of technology availability varies in all cases, from a mathematical model to industrial designs [38–42].

The purpose of this work was to study the catalytic activity and stability during ammonia decomposition of initial materials (LS and LC) and LS–LC composite materials, as well as the structural changes of these materials after the reaction.

2. Experimental

The synthesis of composite catalysts consists of two parts. First, the initial oxide materials LS and LC were synthesized by citrate-nitrate combustion technique through several stages [43]. La_2O_3, Sc_2O_3, Co_3O_4 and $SrCO_3$ (high purity grade) were used as the initial reagents. Co_3O_4 was reduced in a hydrogen atmosphere at a temperature of 650 °C for 4 h to utilize its ability to react with nitric acid. Then stoichiometric amounts of precursors were transferred to a salt solution in interaction with nitric acid, which was mixed with citric acid in a ratio of 2/1 to the amount of the calculated oxide substance and evaporated before the start of the spontaneous combustion process. The prepared powdered materials were calcinated for 1 h at 800 °C. After that, the LS and LC powders were ground in a Retch100 planetary ball mill for 1 h to obtain uniform composition and microstructure. For obtaining single-phase powders, the final synthesis of initial materials was carried out for 2 h at the temperatures, which are need to the phases creation [36, 44], 1350 °C for LS and 1200 °C for LC.

Further, the synthesis of composite materials was carried out by solid-phase mixing of prepared individual materials LS and LC in the following proportions (in mass percentage): 40/60, 50/50 and 60/40 followed by pressing and sintering at 1200 °C for 2 h. Further in the article, a composite with a ratio of 50–50 wt. % will be designated as 50LS–50LC, a composite with a ratio of 60–40 wt. % –60LS–40LC, and a composite with a ratio of 40–60 wt. % –40LS–60LC.

The BET surface area of the support, as-prepared and used catalysts, was determined from the complete nitrogen adsorption isotherms at −196 °C (ASAP 2400 instrument) (Micromeritics, Norcross, USA).

XRD analysis of the obtained powders was carried out on an XRD-6000 diffractometer (Shimadzu, Japan) with Cu-Kα radiation. The diffractograms were recorded in the range of 2θ angles from 20 to 80 °C in a step mode of 0.02 °C with an accumulation time of 0.3 sec. The phase composition of the materials obtained was correlated with the PDF database data.

For elemental analysis, catalyst samples were examined by X-ray fluorescence spectroscopy. The spectrum was recorded on an ARL Perform'X X-ray fluorescence spectrometer (Thermo Scientific™, USA). The spectrum was processed and the content of elements was calculated using the UniQuant Software for Standardless XRF Analysis (Thermo Scientific™, Waltham, USA).

Temperature-programmed reduction (TPR) was conducted on a TG209 F1 Libra Thermo microbalance equipment (Netzsch, Germany). The feed gas He +6 vol. % H_2 flowed at the rate 70 ml/min. The temperature raised linearly from 30 to 800 °C at a rate of 10 °C/min. A QMS 200 gas analyzer (Stanford Research Systems, Sunnyvale, USA) monitored the gas phase composition over the sample.

For shooting in the TEM and STEM modes, a ThemisZ two-corrector transmission electron microscope (Thermo Scientific™, USA) with an accelerating voltage of 200 kV and a limiting resolution of 0.07 nm (TEM) and 0.06 nm (SEM) was used. Micrographs were recorded using a Ceta 16 CCD matrix (Thermo Scientific™, Waltham, USA).

Raman spectra were recorded on a DXR Smart Raman dispersive spectrometer from Thermo Fisher Scientific, equipped with a supplement for recording backscattered light in the range of 52–3417 cm^{-1}. The wavelength of the exciting laser radiation was 780 nm and the laser power was 5 mW. The exposure time was 60 seconds, the number of spectra accumulation was 15. Before recording the Raman spectra, the samples were pressed using a manual press in a special magnetic holder. The Raman spectrum of air was subtracted from the obtained Raman spectra.

IR spectra were recorded on an IR Prestige-21 instrument (Shimadzu, Japan) in the range of 350–7900 °C cm^{-1} with a spectral resolution of 4 cm^{-1}, the number of spectra accumulation was 50. Before recording the spectrum, a small amount of the sample was mixed with KBr powder and pressed into a tablet.

The catalyst activity in the ammonia decomposition was studied in a fixed-bed flow-type reactor at an atmospheric pressure in the temperature range 500–700 °C. The weight of the loaded catalysts was approximately 0.1 g. Pure NH_3 was fed to the reactor at a rate of 60–100 mL/min. The gas mixture at the reactor outlet was analyzed using a Tsvet-500M chromatograph (Tsvet, Russia) with a thermal conductivity detector, and hydrogen as a carrier gas. A column, 1.5 m long, was packed with HayeSep C adsorbent (Hayes Separation, USA), which allows the separation of NH_3 and N_2. The chromatography conditions were as follows: the carrier gas was hydrogen, the flow rate was 60 mL/min, the pressure was 0.1 MPa, the bridge voltage was 4 V, and the column temperature was 70 °C. Based on the data obtained, ammonia conversion and specific catalytic activity (H_2 formation rate, mmol/(g_{cat}·min)) were calculated.

The thermal expansion of the ceramic bars was studied using a quartz dilatometer and Tesatronic TT–80 equipment (TESA, Switzerland) from room temperature to 900 °C with a heating/cooling rate of 2 °C min^{-1} in air.

The electrical resistance was measured by a four-probe DC method using the Hioki RM3545-02 ohmmeter. The samples were formed into parallelepipeds with dimensions of about 12×3×3 mm. The measurements were carried out in the temperature range of 400–900 °C in 50 °C increments using platinum electrodes. Isothermal exposure at each temperature until equilibrium resistance values are reached.

3. Results and discussion

To produce PCFC, it is necessary that the thermal expansion coefficient (TEC) of the materials included in its composition differ from each other by no more than 30%. Therefore, first of all, we carried out measurements of the original materials and all composites based on them (Table S1). The chemical (Table S2) and phase (Fig. S1) composition of the studied materials is presented in supplementary materials. The obtained individual and composite materials were previously studied [45] by the four-probe direct current method to determine electrical conductivity (Fig. S2).

3.1. Specific surface area of La-containing initial materials and composites

According to the BET data, all samples are characterized by a low specific surface area, not typical for ammonia decomposition catalysts (Table 1).

TABLE 1. Specific surface data of individual LS and LC and composite LS–LC materials

Material	S_{BET}, m^2/g	$\sum S_{BET}$, m^2/g^*
LC	5.7	–
LS	3.5	–
40LS–60LC	3.7	4.4
50LS–50LC	4.6	4.6
60LS–40LC	5.6	4.8

* – $\sum S_{BET}$ = S_{BET}(LC)·w(LC)+S_{BET}(LS)·w(LS)

As we can see from the data in Table 1, the specific surface area of composite materials containing a predominant amount of one of the phases differs from the summarize S_{BET} of the materials making up the composite phase. While there is an upward $\sum S_{BET}$ deviation for LC (larger S_{BET}) rich phase, and a downward deviation in LS (smaller S_{BET}) rich phase. XRD data (see. Fig. S1) also show that the initial composite material does not contain phases other than LS and LC. It is known that the characteristic specific surface area of lanthanum cobaltite at calcination temperatures above 800 °C is approximately 10 m^2/g [31]. Using the template synthesis method, mesoporous lanthanum cobaltite with a specific surface area up to 246 m^2/g can be obtained, while the sol-gel synthesis of LC gives S_{BET} 4 m^2/g only [32]. The doping of lanthanum cobaltite by strontium makes it possible to increase the specific surface area by only 50% [25].

3.2. La-containing initial materials and composites properties in ammonia conversion

The catalytic properties of individual LS, LC and LS–LC composite materials in the ammonia decomposition reaction were studied. As shown in Fig. 1, the activity of composite catalysts increases with an increase in the content of a more catalytically active LC phase. Among all the prepared catalysts, the LC catalyst showed the greatest activity, moreover, its activity (Fig. 1) in the entire temperature range is 5–15% higher than that of all other catalysts. The sequential order of catalytic activity of all materials is as follows: LC > 40LS–60LC > 50LS–50LC > 60LS–40LC > LS. This confirms the assumption that the activity of the catalyst is more dependent on the amount of cobalt in the catalyst – the more cobalt, the

more active the catalyst. The presence of the LS phase reduces the activity of composites, which is especially noticeable at low temperatures (500–550 °C), while the activity decreases to a level close to the activity of individual LS. For stability tests, composite materials containing the largest amounts of LC – 50LS–50LC and 60LS–40LC phases, as well as an individual catalytically active LC phase, were selected.

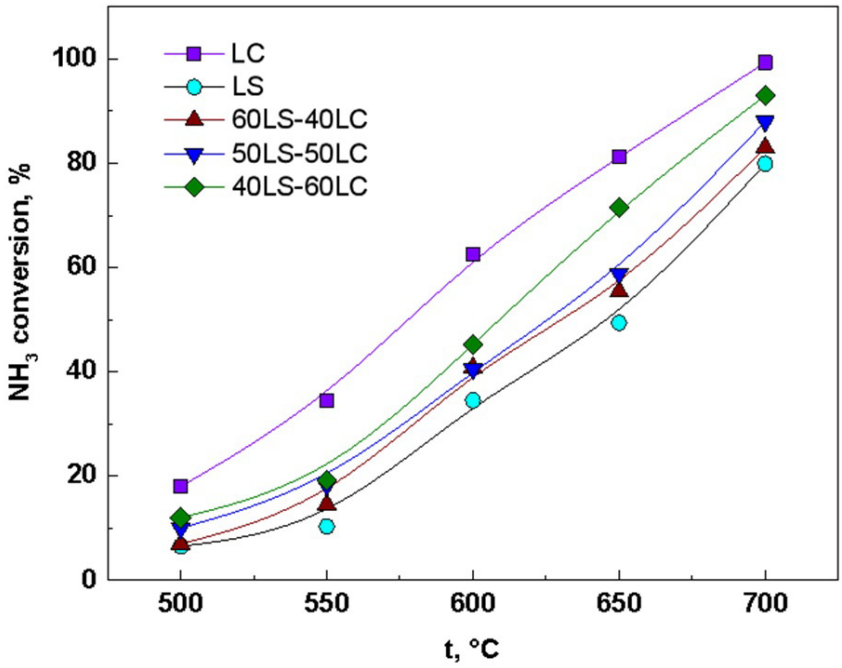

FIG. 1. The influence of the reaction temperature on NH_3 conversion over LS and LC and composite LS–LC materials (GHSV 60000 h^{-1})

3.3. Comparison of the NH_3 decomposition reaction activity of LS, LC and LS–LC composites with the other Co-based ammonia decomposition catalysts

Our composites must operate at working temperatures of PCFCs, equal to 600–700 °C. However, most of NH_3 decomposition cobalt containing catalysts are often very active at 500–600 °C. Therefore, all catalysts investigated in this work were compared at 550 °C. It can be seen from Table 2 that at 550 °C, LC is inferior to all other catalysts in terms of NH_3 conversion, but exceeds them in H_2 formation rate. Note, the catalysts from the referent investigations presented in Table 2 are used only for direct NH_3 decomposition not for ammonia PCFC (except of 1%Ni-9%Co/$Ce_{0.6}Zr_{0.3}Y_{0.1}O_2$). But it is necessary for 50LS–50LC composite have the specific electrical and mechanical properties for use in PCFC, and the optimum in these properties is achieved at as small specific surface area as 4.6 m^2/g. At the same time, the specific surface area of the most active NH_3 decomposition catalysts is significantly higher: $LaCoO_x$/Co@NC/SBA-15(2D) – 259 m^2/g [20], 20%Co/$LaMgO_x$ – 89 m^2/g [33].

3.4. Catalyst life tests for La-containing initial materials and composites

To study the changes in LC, 50LS–50LC and 60LS–40LC composites under the influence of a reaction medium, catalytic resistance tests were carried out (Fig. 2). Experiments have shown that at a reaction temperature of 700 °C, LC showed maximum activity, which remained stable throughout the entire test period (40 h). It was found that the introduction of LS reduces the activity, while the stability of the 40% LS sample decreases slightly. When the proportion of LS increases to 50%, the sample loses activity and is characterized by the lowest conversion rate (87%) compared to the rest of the samples in this series. It was found that in this sample, the conversion rate decreases during the first 7 hours from 87 to 85% and then stabilizes.

3.5. The transformation of La-containing composites in ammonia decomposition conditions

To explain the reasons for the increase in catalyst activity with increasing LC phase content, the synthesized samples were studied using a number of methods. So, according to TPR data (Fig. S3), in the presence of hydrogen, the cobalt (III), which is present in the LC phase, is reduced to Co (II) at a temperature of 400 °C and, further, it is transformed to metal at heating above 600 °C. The similar cobalt reduction processes can occur also in hydrogen-rich real ammonia decomposition reaction medium at 600–700 °C.

Indeed, the TEM results for the 50LS–50LC sample (Fig. 3) confirm that the initial sample is a mixture of two perovskite-like oxide phases, evenly spaced relative to each other. LS perovskite particles have a round shape with an

TABLE 2. Comparison of the NH_3 decomposition reaction activity of individual LS and LC as well as LS–LC composite catalyst with the reported Co-based catalysts

Catalyst	WHSV ($cm^3g^{-1}h^{-1}$	Temp. (°C)	NH_3 conversion (%)	H_2 Form. Rate (mmol g^{-1} min^{-1})	Ref.
LC	60000	550	34.4	23.0	This work
LC	60000	700	99.3	66.5	This work
LC	12000	700	100	13.4	This work
LS	60000	550	10.3	6.9	This work
LS	60000	700	79.9	53.5	This work
LS	12000	700	98.1	13.1	This work
50LS–50LC	60000	550	18.2	12.2	This work
40LS–60LC	60000	550	19.2	12.8	This work
60LS–40LC	60000	550	14.6	9.7	This work
$LaCoO_x$/Co@NC/SBA–15(2D)	30000	550	99.9	33.5	[20]
5%Co/MgO–5La_2O_3	6000	550	82.7	5.5	[21]
5%Co/MgO–2CeO_2	6000	550	69.1	4.6	[21]
5%Co/$MgLaO_x$–N_2	6000	550	91	6.1	[22]
20%Co/$LaMgO_x$	124000	550	64	91	[33]
NiCo/LST on $Sm_{0.2}Ce_{0.8}O_{1.9}$	3000*	600	18	0.6	[46]
NiCo/LST on $Sm_{0.2}Ce_{0.8}O_{1.9}$	3000*	700	56	1.88	[46]
90CoAl	18000	550	90	18.1	[47]
1%Ni–9%Co/ $Ce_{0.6}Zr_{0.3}Y_{0.1}O_2$	6000	550	89	6.0	[48]
1%Ni–9%Co/ $Ce_{0.6}Zr_{0.3}Y_{0.1}O_2$	48000	700	99	53.0	[48]
Co–Mo–Air–750	36000	550	38	15.3	[49]

* WHSV is given in terms of ammonia, for all gas mixtures 10 ml/min NH_3 and 80 ml/min Ar WHSV was 27000 gas/(g_{cat}·h)

average crystallite size of about 200 nm, and the second material is presented in the form of dendrite-like agglomerates of particles with sizes of 100–500 nm, consisting of crystallites with sizes of about 50–100 nm. Using HRTEM it was shown that the surface of both materials is enriched with cobalt oxide particles with an average size of 3–10 nm. In addition, EDX mapping showed that part of the LC surface is covered with a layer of Sr oxide.

According to electronic mapping data (Supplementary materials, Table S3), lanthanum, strontium and oxygen are distributed over the entire surface of the sample, the areas enriched in cobalt correspond to the LC phase and the high scandium concentration areas correspond to the LS phase. The atomic ratio La : O is 1 : 2.5, which is close to the ratio of the amounts of these elements in the phases to be consisted the composite. The atomic ratio of Sr : O is 0.04 : 1, which is also close to the ratio of these elements in the LC and LS phases, in which strontium should be present in the same amount. The atomic ratio of cobalt and oxygen concentrations, according to elemental mapping data, is 0.18 : 1 that confirms the presence of both LC and LS phases in the sample in equal amounts, since according to the above formulas, in the LC phase the Co : O ratio is approximately 0.33 : 1, and in the LS phase, this ratio is about 0.033 : 1. The ratio of scandium and oxygen concentrations is 0.26 : 1, which is slightly lower, but also close to the ratio of the amounts of these elements in the LS phase.

To explain the reasons for the increased activity of the catalyst with an increase in the LC phase content, the synthesized samples were studied using a number of methods. So, according to the TPR data (the results are presented in supplementary materials), in the presence of hydrogen, cobalt (III) present in the LC phase is reduced to Co (II) at a temperature of 400 °C and further converted to metal when heated above 600 °C. Similar cobalt reduction processes can also take place in a real hydrogen-rich reaction medium in PCFC at a temperature of 600–700 °C.

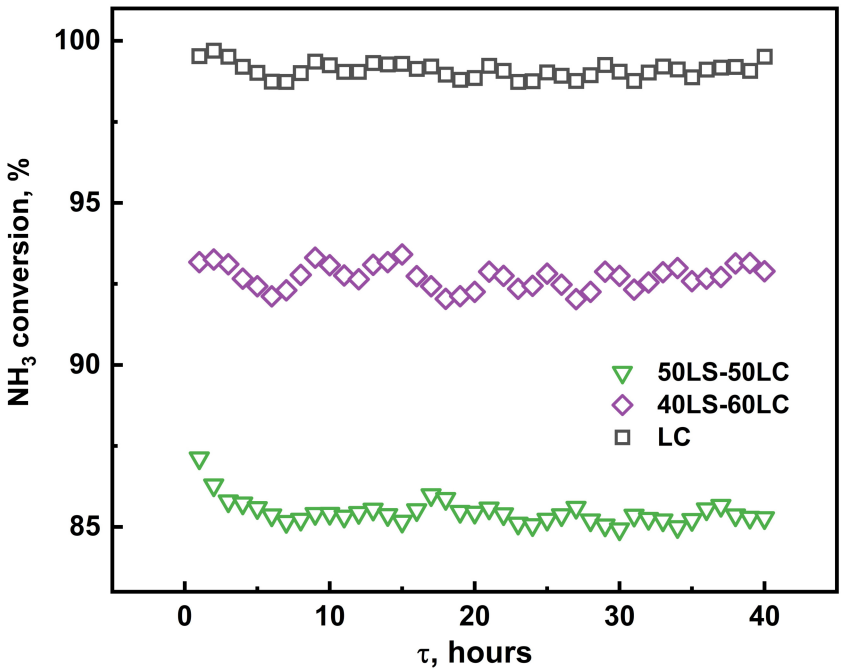

FIG. 2. Catalyst life tests for 50LS–50LC, 40LS–60LC and LC (GHSV 60000 h^{-1}) for 700 °C

Indeed, the results of the study of sample 50 LS–50LC using TEM (Fig. 3) confirm that the initial sample is a mixture of two perovskite-like oxides evenly spaced relative to each other. LS perovskite particles have a round shape with an average crystallite size of about 200 nm, and the second oxide is represented as dendrite-like agglomerates of particles with a size of 100–500 nm, consisting of crystallites with a size of about 50–100 nm. Using HRTEM, it was shown that the surface of both oxides is enriched with cobalt oxide particles with an average size of 3–10 nm. In addition, EDX mapping showed that part of the LC surface is covered with a layer of Sr oxide.

According to the electronic mapping data (supplementary materials, tables S3, S4), lanthanum, strontium and oxygen are distributed over the entire surface of the sample, areas enriched with cobalt correspond to the LC phase, and areas with a high concentration of scandium correspond to the LS phase. The atomic ratio of La : O is 1 : 2.5, which is close to the ratio of the amounts of these elements in the phases that make up the composite. The atomic ratio of Sr : O is 0.04 : 1, which is also close to the ratio of these elements in the LC and LS phases, in which strontium should be present in the same amount. The atomic ratio of cobalt and oxygen concentrations, according to elemental mapping data, is 0.18 : 1, which confirms the presence of both LC and LS phases in the sample in equal quantities, since according to the above formulas, the LC phase has a Co ratio: O is approximately 0.33 : 1, and in the LS phase this ratio is about 0.033 : 1. The ratio of scandium and oxygen concentrations is 0.26 : 1, which is slightly lower, but also close to the ratio of the amounts of these elements in the LS phase.

During the testing the composite material in ammonia decomposition, the perovskite-like oxide LC is destroyed, and the binary phase system $La(OH)_3$ and metallic cobalt are formed (Fig. 4). In this case, Co particles are located in the lanthanum hydroxide matrix and have sizes of 20–40 nm. The average particle size of $La(OH)_3$ is 100–200 nm. The crystal lattice of perovskite oxide LS does not have significant changes.

3.6. The changes occurring in the composites confirmed by IR and Raman spectroscopy methods

If LS and LC have a crystal structure with a space symmetry group Pnma as established from X-ray diffraction data, then Raman spectra should be free of any normal vibrations [50]. The results obtained confirm this assertion (Fig. 5). The Raman spectrum of the sample 50LS–50LC exposed to the ammonia decomposition reaction medium contains a band at 688 cm^{-1}. The results obtained indicate the destruction of the original crystal structure of the samples studied due to the removal of CoO_4 structural units from the unit cell in reducing medium. In addition, the appearance of additional signals observed in the Raman spectrum of the sample after reaction, apparently related to the fiberglass used in catalytic tests. Thus, it can be assumed that in an ammonia environment the crystal structure of the LC sample is destroyed.

IR spectrum of the initial LC sample (Fig. 6) has an intense absorption band at 593 cm^{-1}, which related to the stretching vibrations of Co-O bonds in octahedral coordination [51–53]. A low intensity absorption band at 549 cm^{-1} related to stretching vibrations of La(Sr)–O bonds was also observed in the IR-spectrum of this sample. In addition, an absorption band at 409 cm^{-1} appears in the IR spectrum that related to stretching vibrations of La–O bonds in dodecahedral coordination. New absorption bands at 3610 and 652 cm^{-1} appears in the IR spectrum of LC after the testing in

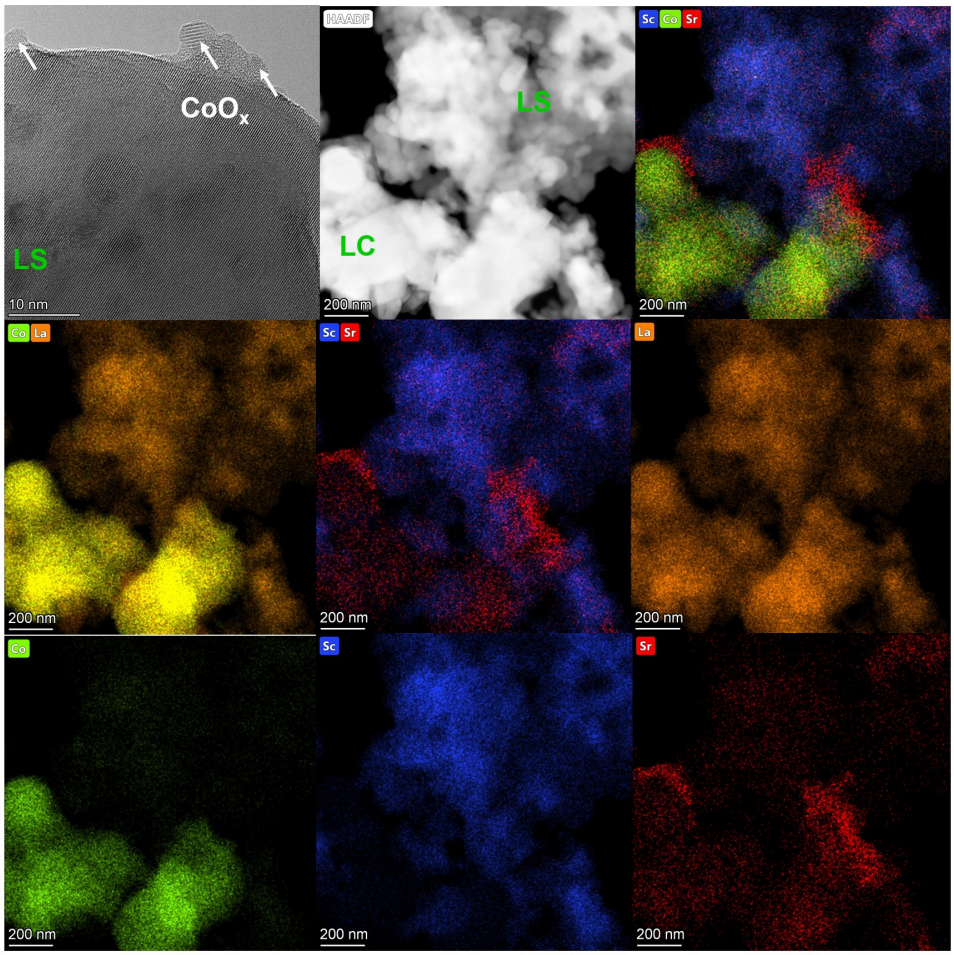

FIG. 3. HRTEM images of the 50LS–50LC sample in the initial state. The white arrows show CoO_x

ammonia decomposition (Fig. 6) that corresponding to the stretching vibrations of O–H bonds and strain vibrations of La-OH bonds in the $La(OH)_3$ structure [54]. In addition, the absorption bands at 386 and 472 cm^{-1} corresponding to the fundamental vibrations of La–O bonds recorded in the IR spectrum of this sample.

The IR spectrum of initial LS has intense absorption bands at 375 and 536 cm^{-1}, which correspond to the stretching vibrations of the Sc–O and La(Sr)–O bonds. In contradistinction to LC, no significant changes observed in the IR spectrum of the LS sample after the testing in ammonia decomposition. An intense absorption band is observed at 595 cm^{-1} in the IR spectrum of the 50LS–50LC initial composite that corresponding to stretching vibrations of Co–O bonds in octahedral coordination. But in IR spectrum of a composite sample exposed to ammonia decomposition reaction medium absorption bands at 3610 and 649 cm^{-1}, corresponding to stretching vibrations of OH bonds and strain vibrations of La-OH bonds in the $La(OH)_3$ structure appears. In addition, absorption bands at 378 and 539 cm^{-1}, which are typical of the LS sample, observed in IR spectrum of the composite after the testing in ammonia decomposition.

We chose one of the most stable LC compositions, which does not decompose into different phases under oxidizing conditions at a temperature of 700 °C [55]. However, in this work we have shown that the same composition under reducing conditions is unstable.

To clarify the question of what happens to the structure of the LS and LC phases upon prolonged exposure to the reaction medium, the samples were studied by X-ray diffraction (Fig. 7). According to XRD, after the testing in decomposition of ammonia the formation of metallic cobalt and lanthanum hydroxide is observed. This phenomenon has been observed in catalysts based on magnesium lanthanum oxides [33].

The initial La-containing composites is a two-phase system consisting of $LaCoO_3$ [PDF 25-1060] and $LaScO_3$ [PDF 26-1148]. La-containing composites tested in the ammonia decomposition are characterized by the presence of $LaScO_3$ [PDF 26-1148], $La(OH)_3$ [PDF 36-1481] and cobalt [PDF 15-0806] phases. The formation of the $La(OH)_3$ phase under the decomposition of ammonia is very typical for catalysts containing lanthanum oxide as a support [20, 22, 33].

Thus, we can conclude that in the reaction medium the structures of both the individual LC sample and this phase in the LS–LC composite are destroyed, with the formation of $La(OH)_3$ and cobalt. The LS phase does not undergo significant changes and serves as a reinforcing frame that prevents mechanical destruction of the particles of the active component.

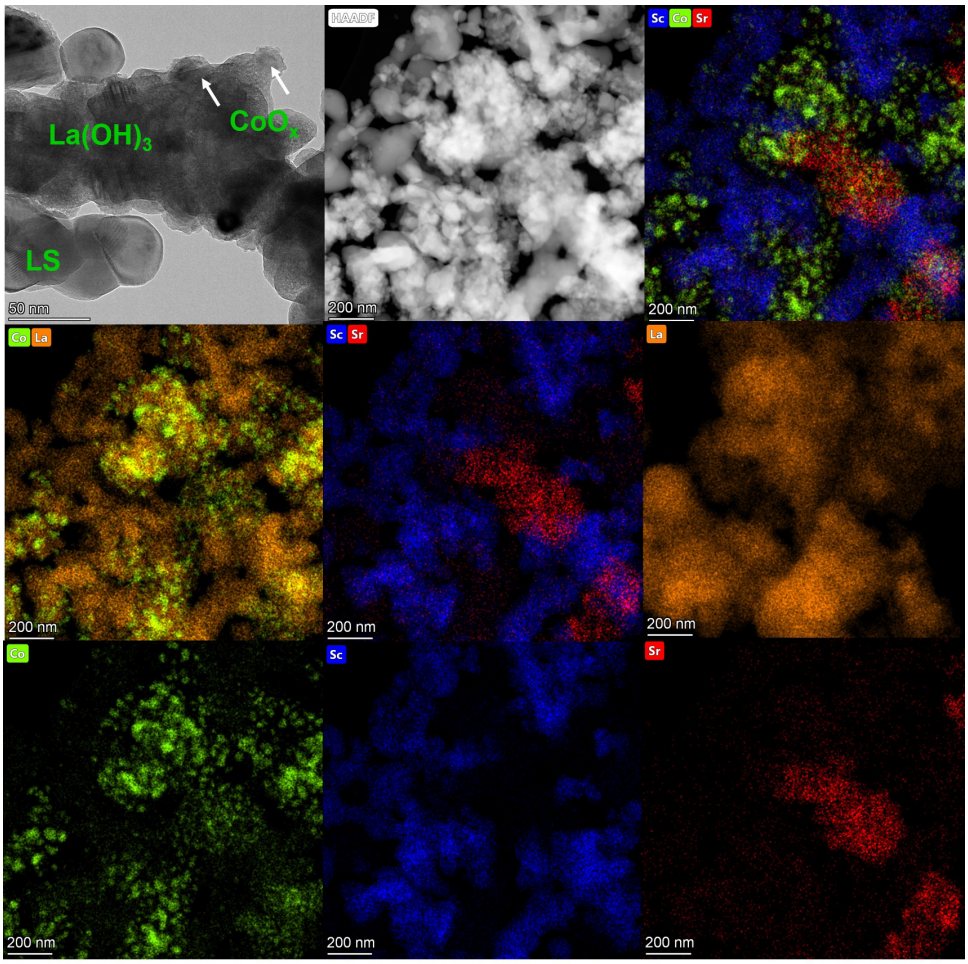

FIG. 4. HRTEM images of the 50LS–50LC sample after reaction

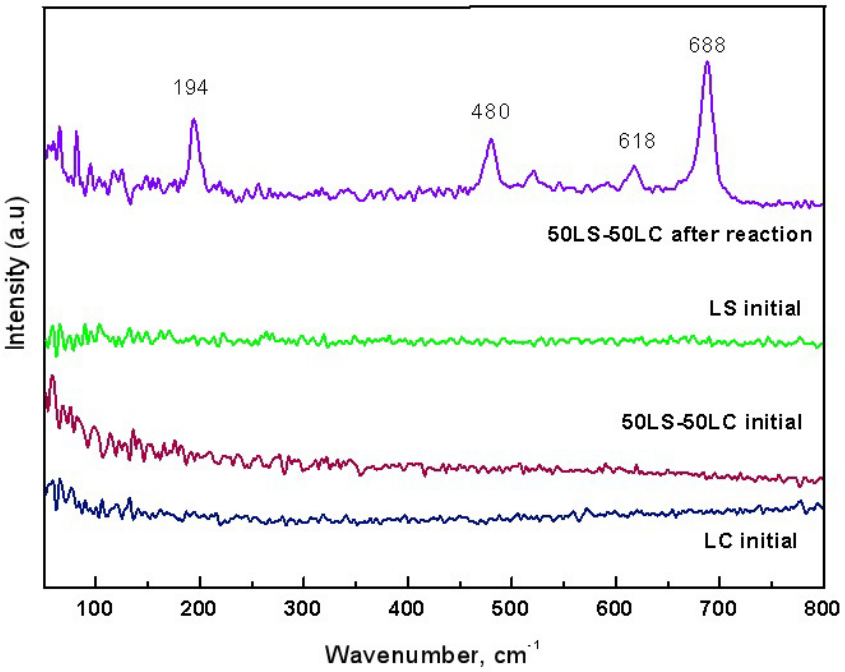

FIG. 5. Raman spectra of the La-containing materials and composites

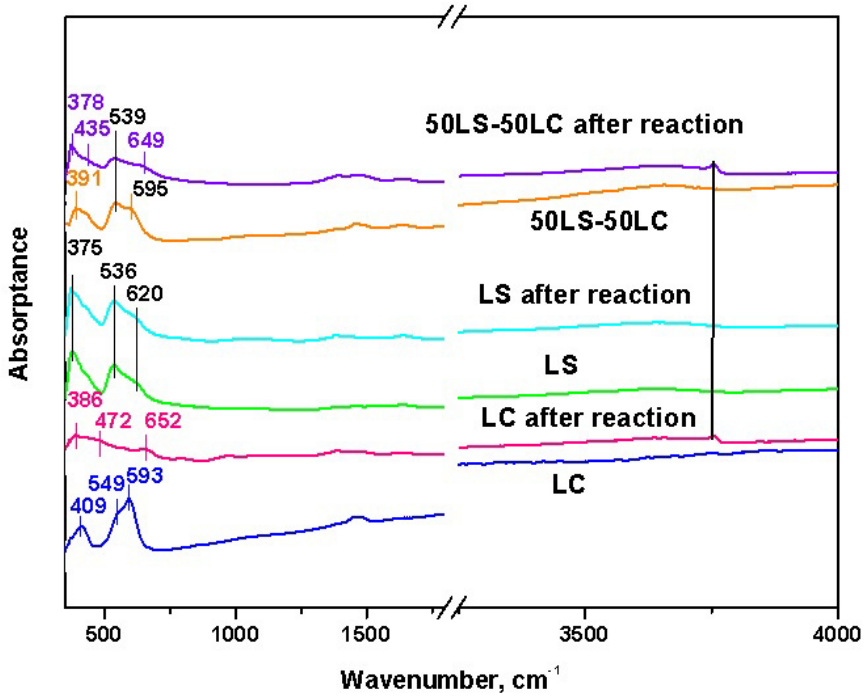

FIG. 6. IR spectra of the La-containing initial materials and composites

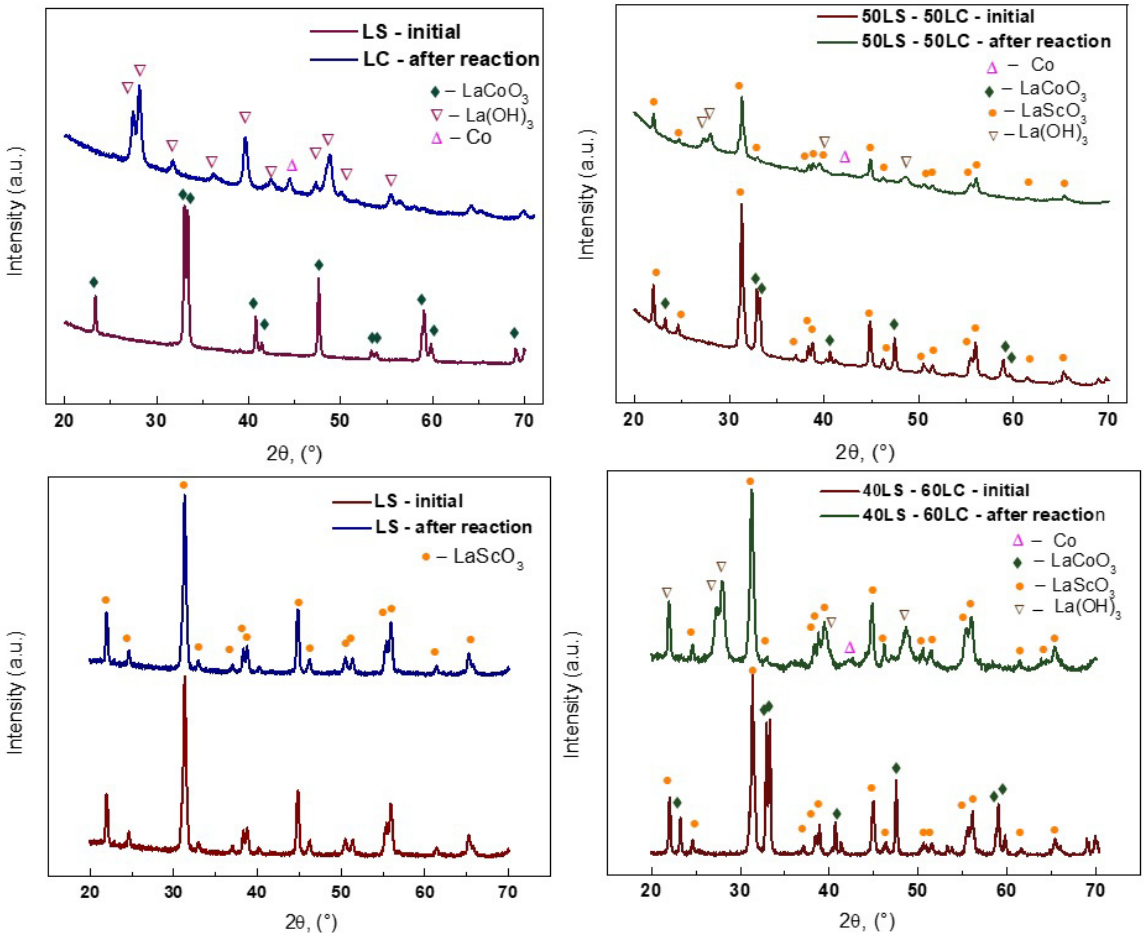

FIG. 7. XRD data for initial La-containing materials/composites and La-containing materials/composites after testing in ammonia decomposition reaction

As can be seen at 700 °C (PCFC operating temperature), our catalysts are quite active compared to other PCFC materials (for example, NiCo/LST on $Sm_{0.2}Ce_{0.8}O_{1.9}$). It is also clear that non-standard materials can be used here, which are usually not used as an anode, for example, LS, LC and composites based on them. According to the results of XRD, RAMAN, IR spectroscopy and TEM, it can be seen that the LS phase is quite stable in an ammonia environment, but most importantly, it is perfectly compatible with the electrolyte, which will help simplify the design of the PCFC.

4. Conclusions

The LS and LC phases and composite materials based on them, promising for use in PCFC running on ammonia, have been synthesized. The best result in the decomposition of ammonia at 700 °C and WHSV of 60,000 ml $NH_3 \cdot g_{cat}^{-1} \cdot h^{-1}$ shows LC – 99%, the worst LS – 80%. Under the conditions of a stability experiment which is carried out also at a temperature of 700 °C and WHSV of 60,000 ml $NH_3 \cdot g_{cat}^{-1} \cdot h^{-1}$, the degree of ammonia conversion reaches 99% in LC, and 93% in 40LS–60LC, and in 50LS–50LC composite decreases from 87 to 85 % during the first 7 hours and remains unchanged for 40 hours.

Also, it was found that under the influence of a reaction medium, the LC phase decays to form cobalt and $La(OH)_3$ nanoparticles. These data are confirmed by the results of XRD, IR, Raman and TEM studies. In the sample after the test, during the decomposition of ammonia, according to XRD data, characteristic peaks of $La(OH)_3$ are observed, as evidenced also by the IR absorption band at 3610 cm^{-1}. The presence of the active component, cobalt, is confirmed by XRF and TEM data. At the same time, according to the PEM data, the LS phase does not undergo significant changes.

References

[1] Abe J.O., Popoola A.P.I., Ajenifuja E., Popoola O.M. Hydrogen energy, economy and storage: Review and recommendation. *Int J Hydrogen Energy.*, 2019, **44**(29), P. 15072–15086.

[2] Yan Z., Yin K., Xu M., Fang N., Yu W., Chu Y., et al. Photocatalysis for synergistic water remediation and H2 production: A review. *Chem Eng J.*, 2023, **472**, P. 145066.

[3] Aravindan M., Praveen Kumar G. Hydrogen towards sustainable transition: A review of production, economic, environmental impact and scaling factors. *Results Eng.*, 2023, **20**, P. 101456.

[4] El-Shafie M. Hydrogen production by water electrolysis technologies: A review. *Results Eng.*, 2023, **20**, P. 101426.

[5] Egerer J., Grimm V., Niazmand K., Runge P. The economics of global green ammonia trade – "Shipping Australian wind and sunshine to Germany." *Appl Energy*, 2023, **334**, P. 120662.

[6] Wang B., Ni M., Jiao K. Green ammonia as a fuel. *Sci Bull.*, 2022, **67**(15), P. 1530–1534.

[7] Jiang L., Fu X. An Ammonia–Hydrogen Energy Roadmap for Carbon Neutrality: Opportunity and Challenges in China. *Engineering*, 2021, **7**(12), P. 1688–1691.

[8] Borisov V.A., Sidorchik I.A., Temerev V.L., Simunin M.M., Leont'eva N.N., Muromtsev I.V., et al. Ru-Ba/ANF catalysts for ammonia decomposition: Support carbonization influence. *Int J Hydrogen Energy*, 2023, **48**(59), P. 22453–22461.

[9] Hayashi F., Toda Y., Kanie Y., Kitano M., Inoue Y., Yokoyama T., et al. Ammonia decomposition by ruthenium nanoparticles loaded on inorganic electride C12A7:e-. *Chem Sci.*, 2013, **4**(8), P. 3124–3130.

[10] Kocer T., Oztuna F.E.S., Kurtoğlu S.F., Unal U., Uzun A. Graphene aerogel-supported ruthenium nanoparticles for COx-free hydrogen production from ammonia. *Appl Catal A Gen.*, 2021, **610**, P. 117969.

[11] Borisov V.A., Iost K.N., Temerev V.L., Simunin M.M., Leont'eva N.N., Mikhlin Y.L., et al. Ammonia decomposition Ru catalysts supported on alumina nanofibers for hydrogen generation. *Mater Lett.*, 2022, **306**, P. 130842.

[12] Borisov V.A., Iost K.N., Temerev V.L., Leont'eva N.N., Muromtsev I.V., Arbuzov A.B., et al. The Influence of the Specific Surface Area of the Carbon Support on the Activity of Ruthenium Catalysts for the Ammonia-Decomposition Reaction. *Kinet Catal.*, 2018, **59**(2), P. 136–142.

[13] Borisov V.A., Iost K.N., Petrunin D.A., Temerev V.L., Muromtsev I.V., Arbuzov A.B., et al. Effect of the Modifier on the Catalytic Properties and Thermal Stability of Ru–Cs(Ba)/Sibunit Catalyst for Ammonia Decomposition. *Kinet Catal.*, 2019, **60**, P. 372–379.

[14] Yamazaki K., Matsumoto M., Ishikawa M., Sato A. NH_3 decomposition over Ru/CeO_2-PrOx catalyst under high space velocity conditions for an on-site H_2 fueling station. *Appl Catal B Environ*, 2023, **325**, P. 122352.

[15] Le T.A., Do Q.C., Kim Y., Kim T.-W., Chae H.-J. A review on the recent developments of ruthenium and nickel catalysts for CO_x-free H_2 generation by ammonia decomposition. *Korean J. Chem Eng.*, 2021, **38**(6), P. 1087–1103.

[16] Sun S., Jiang Q., Zhao D., Cao T., Sha H., Zhang C., et al. Ammonia as hydrogen carrier: Advances in ammonia decomposition catalysts for promising hydrogen production. *Renew Sustain Energy Rev.*, 2022, **169**, P. 112918.

[17] Bell T.E., Torrente-Murciano L. H_2 Production via Ammonia Decomposition Using Non-Noble Metal Catalysts: A Review. *Top Catal.*, 2016, **59**(15), P. 1438–1457.

[18] Lucentini I., Garcia X., Vendrell X., Llorca J. Review of the Decomposition of Ammonia to Generate Hydrogen. *Ind Eng Chem Res.*, 2021 May, **60**(51), P. 18560–18611.

[19] Yakovenko R.E., Krasnyakova T.V., Saliev A.N., Shilov M.A., Volik A.V., Savost'yanov A.P., et al. Ammonia Decomposition over Cobalt-Based Silica-Supported Fischer-Tropsch Synthesis Catalysts. *Kinet Catal.*, 2023, **64**(2), P. 180–190.

[20] Han X., Hu M., Yu J., Xu X., Jing P., Liu B., et al. Dual confinement of $LaCoO_x$ modified Co nanoparticles for superior and stable ammonia decomposition. *Appl Catal B Environ.*, 2023, **328**, P. 122534.

[21] Podila S., Alhamed Y.A., AlZahrani A.A., Petrov L.A. Hydrogen production by ammonia decomposition using Co catalyst supported on Mg mixed oxide systems. *Int. J. Hydrogen Energy.*, 2015, **40**(45), P. 15411–15422.

[22] Podila S., Driss H., Zaman S.F., Alhamed Y.A., AlZahrani A.A., Daous M.A., et al. Hydrogen generation by ammonia decomposition using Co/MgO–La_2O_3 catalyst: Influence of support calcination atmosphere. *J. Mol. Catal. A Chem.*, 2016, **414**, P. 130–139.

[23] Chandrappa S.G., Moni P., Chen D., Karkera G., Prakasha K.R., Caruso R.A., et al. The influence of ruthenium substitution in $LaCoO_3$ towards bi-functional electrocatalytic activity for rechargeable Zn–air batteries. *J Mater Chem A.* 2020, **8**(39), P. 20612–20620.

[24] Onrubia-Calvo J.A., Pereda-Ayo B., De-La-Torre U., González-Velasco J.R. Key factors in Sr-doped $LaBO_3$ (B = Co or Mn) perovskites for NO oxidation in efficient diesel exhaust purification. *Appl Catal B Environ.*, 2017, **213**, P. 198–210.

[25] Wei Y., Ni L., Li M., Zhao J. Acid treated Sr-substituted $LaCoO_3$ perovskite for toluene oxidation. *Catal Commun.*, 2021, **155**, P. 106314.
[26] Wang S., Zhu J., Yang J., Li M., Zhu Y. Influence of $LaCoO_3$ perovskite oxides prepared by different method on the catalytic combustion of ethyl acetate in the presence of NO. *Appl Surf Sci.*, 2023, **623**, P. 157045.
[27] Ao R., Ma L., Guo Z., Liu H., Yang J., Yin X., et al. Effects of the preparation method on the simultaneous catalytic oxidation performances of $LaCoO_3$ perovskites for NO and Hg0. *Fuel*, 2021, **305**, P. 121617.
[28] Li P., Chen X., Li Y., Schwank J.W. Effect of preparation methods on the catalytic activity of $La_{0.9}Sr_{0.1}CoO_3$ perovskite for CO and C_3H_6 oxidation. *Catal Today*, 2021, **364**, P. 7–15.
[29] Yan F., Li P., Zhang X. CO and C_3H_6 oxidation over $La_{0.9}Sr_{0.1}CoO_3$ catalysts: Influence of preparation solvent. *Korean J Chem Eng.*, 2021, **38**(5), P. 945–951.
[30] Zhao D., Song H., Liu J., Jiang Q., Li X., Xie W., et al. Advances in Designing Efficient La-Based Perovskites for the NOx Storage and Reduction Process. *Catalysts*, 2022, **431**(6), P. 128528.
[31] Saifei Wang, Yiyuan Zhang, Peiqi Chu, Jie Liu, Man Wang, Peng Zhang, et al. Different Active Sites of $LaCoO_3$ and $LaMnO_3$ for CH_4 Oxidation by Regulation of Precursor's Ion Concentration. *Glob Environ Eng.*, 2020 Sep, **7**(1 SE-Articles), P. 28–39.
[32] Xie W., Xu G., Zhang Y., Yu Y., He H. Mesoporous $LaCoO_3$ perovskite oxide with high catalytic performance for NOx storage and reduction. *J Hazard Mater.*, 2022, **431**, P. 128528.
[33] Hu X.-C., Wang W.-W., Jin Z., Wang X., Si R., Jia C.-J. Transition metal nanoparticles supported La-promoted MgO as catalysts for hydrogen production via catalytic decomposition of ammonia. *J. Energy Chem.*, 2019, **38**, P. 41–49.
[34] Wojcik A., Middleton H., Damopoulos I., Van herle J. Ammonia as a fuel in solid oxide fuel cells. *J. Power Sources.*, 2003, **118**(1), P. 342–348.
[35] Yang J., Molouk A.F.S., Okanishi T., Muroyama H., Matsui T., Eguchi K. Electrochemical and Catalytic Properties of Ni/$BaCe_{0.75}Y_{0.25}O_3$-δ Anode for Direct Ammonia-Fueled Solid Oxide Fuel Cells. *ACS Appl Mater Interfaces.*, 2015 Apr, **7**(13), P. 7406–7412.
[36] Plekhanov M.S., Kuzmin A.V., Tropin E.S., Korolev D.A., Ananyev M.V., New mixed ionic and electronic conductors based on $LaScO_3$: Protonic ceramic fuel cells electrodes. *J. Power Sources.*, 2020, **449**, P. 227476.
[37] Wang B., Li T., Gong F., Othman M.H.D., Xiao R. Ammonia as a green energy carrier: Electrochemical synthesis and direct ammonia fuel cell – a comprehensive review. *Fuel Process Technol.*, 2022, **235**, P. 107380.
[38] Rahman M.M., Abdalla A.M., Omeiza L.A., Raj V., Afroze S., Reza M.S., et al. Numerical Modeling of Ammonia-Fueled Protonic-Ion Conducting Electrolyte-Supported Solid Oxide Fuel Cell (H-SOFC). *A Brief Review.*, 2023, **11**(9), P. 2728.
[39] Mehdi A.M., Hussain A., Khan M.Z., Hanif M.B., Song R.-H., Kazmi W.W., et al. Progress and prospects in direct ammonia solid oxide fuel cells. *Russ Chem Rev.*, 2023, **92**(11), RCR5098.
[40] Quach T.-Q., Sang Kim Y., Keun Lee D., Young Ahn K., Lee S., Bae Y. Thermal management of Ammonia-fed Solid oxide fuel cells using a novel alternate flow interconnector. *Energy Convers Manag.*, 2023, **291**, P. 117248.
[41] Quach T.-Q., Lee D., Giap V.-T., Kim Y.S., Lee S., Ahn K.Y. Energetic and economic analysis of novel cascade systems for ammonia-fed solid oxide fuel cell. *Int J Hydrogen Energy*, 2024, **67**, P. 1080–96.
[42] Quach T.-Q., Giap V.-T., Keun Lee D., Pineda Israel T., Young Ahn K. High-efficiency ammonia-fed solid oxide fuel cell systems for distributed power generation. *Appl Energy*, 2022, **324**, P. 119718.
[43] Kuzmin A.V., Stroeva A.Y., Gorelov V.P., Novikova Y.V., Lesnichyova A.S., Farlenkov A.S., et al. Synthesis and characterization of dense proton-conducting $La_{1-x}Sr_xScO_3$-α ceramics. *Int J Hydrogen Energy*, 2019, **44**(2), P. 1130–1138.
[44] Gwon O., Yoo S., Shin J., Kim G. Optimization of $La_{1-x}Sr_xCoO_3$-δ perovskite cathodes for intermediate temperature solid oxide fuel cells through the analysis of crystal structure and electrical properties. *Int J Hydrogen Energy*, 2014, **39**(35), P. 20806–20811.
[45] Stroeva A.Y., Ichetovkin Z.N., Plekhanov M.S., Borisov V.A., Shlyapin D.A., Snytnikov P.V., et al. The Lanthanum-Scandate- and Lanthanum-Cobaltite-Based Composite Materials for Proton–Ceramic Electrochemical Devices. *Russ. J. Electrochem*, 2024, **60**(1), P. 36–43.
[46] Song Y., Li H., Xu M., Yang G., Wang W., Ran R., et al. Infiltrated NiCo Alloy Nanoparticle Decorated Perovskite Oxide: A Highly Active, Stable, and Antisintering Anode for Direct-Ammonia Solid Oxide Fuel Cells. *Small*, 2020 Jul, **16**(28), P. 2001859.
[47] Zhang Z.-S., Fu X.-P., Wang W.-W., Jin Z., Song Q.-S., Jia C.-J. Promoted porous Co_3O_4–Al_2O_3 catalysts for ammonia decomposition. *Sci China Chem.*, 2018, **61**(11), P. 1389–1398.
[48] Huang C., Li H., Yang J., Wang C., Hu F., Wang X., et al. $Ce_{0.6}Zr_{0.3}Y_{0.1}O_2$ solid solutions-supported NiCo bimetal nanocatalysts for NH_3 decomposition. *Appl Surf Sci.*, 2019, **478**, P. 708–716.
[49] Duan X., Ji J., Yan X., Qian G., Chen D., Zhou X. Understanding Co-Mo Catalyzed Ammonia Decomposition: Influence of Calcination Atmosphere and Identification of Active Phase. *Chem.Cat.Chem.*, 2016 Mar, **8**(5), P. 938–945.
[50] Breucop J.D. In Situ Raman Spectroscopy of Lanthanum- Strontium-Cobaltite Thin Films. By Department of Materials Science and Engineering at the Massachusetts Institute of Technology. 2012, 36 p.
[51] Dragan M., Enache S., Varlam M., Petrov K. Perovskite-Type Lanthanum Cobaltite $LaCoO_3$: Aspects of Processing Route toward Practical Applications. In: Yɀldɪz Y, Manzak A, editors. *Rijeka: IntechOpen*, 2019, Ch. 6.
[52] Wandekar R.V., Wani B.N., Bharadwaj S.R. Crystal structure, electrical conductivity, thermal expansion and compatibility studies of Co-substituted lanthanum strontium manganite system. *Solid State Sci.*, 2009, **11**(1), P. 240–250.
[53] Petrov A.N., Kononchuk O.F., Andreev A.V., Cherepanov V.A., Kofstad P. Crystal structure, electrical and magnetic properties of $La_{1-x}Sr_xCoO_{3-y}$. *Solid State Ionics.*, 1995, **80**(3), P. 189–199.
[54] Li G., Yu X., Yin F., Lei Z., Zhang H., He X. Production of hydrogen by ammonia decomposition over supported Co_3O_4 catalysts. *Catal Today.*, 2022, **402**, P. 45–51.
[55] Zhang W.-W., Povoden-Karadeniz E., Shang Y., Hendriksen P.V., Chen M. Phase equilibria and defect chemistry of the La–Sr–Co–O system. *J Eur Ceram Soc.*, 2023, **43**(10), P. 4419–4430.

Submitted 8 June 2025; accepted 22 June 2025

Information about the authors:

Vadim A. Borisov – Center of New Chemical Technologies BIC, Boreskov Institute of Catalysis, Neftezavodskaya st., 54, Omsk, 644040, Russia; ORCID 0000-0001-6289-8029; borisovtiger86@mail.ru

Zaliya A. Fedorova – Boreskov Institute of Catalysis, Lavrentiev Ave., 5, Novosibirsk, 630090, Russia; ORCID 0000-0003-1374-5557; sabirova@catalysis.ru

Zakhar N. Ichetovkin – Department of Technology of Inorganic Materials and Electrochemical Production, Vyatka State University, Moskovskaya st., 36, Kirov, 610000, Russia; Institute of Solid State Chemistry and Mechanochemistry of the Siberian Branch of the RAS, Kutateladze st., 18, Novosibirsk, 630128, Russia; ORCID 0009-0008-0370-4528; zakhar1030@mail.ru

Evgeniy Y. Gerasimov – Boreskov Institute of Catalysis, Lavrentiev Ave., 5, Novosibirsk, 630090, Russia; ORCID 0000-0002-3230-3335; gerasimov@catalysis.ru

Dmitry A. Shlyapin – Boreskov Institute of Catalysis, Lavrentiev Ave., 5, Novosibirsk, 630090, Russia; ORCID 0000-0001-6280-9292; dmitryshlyapin@yandex.ru

Anna Y. Stroeva – Department of Technology of Inorganic Materials and Electrochemical Production, Vyatka State University, Moskovskaya st., 36, Kirov, 610000, Russia; ORCID 0000-0002-6772-3321; stroevaanna@yandex.ru

Victor L. Temerev – Center of New Chemical Technologies BIC, Boreskov Institute of Catalysis, Neftezavodskaya st., 54, Omsk, 644040, Russia; ORCID 0000-0002-4524-4178; tvl@ihcp.ru

Alexey B. Arbuzov – Center of New Chemical Technologies BIC, Boreskov Institute of Catalysis, Neftezavodskaya st., 54, Omsk, 644040, Russia; ORCID 0000-0003-1847-6544; arbuzov@ihcp.ru

Sergey V. Tsybulya – Boreskov Institute of Catalysis, Lavrentiev Ave., 5, Novosibirsk, 630090, Russia; ORCID 0000-0003-1038-6018; tsybulya@catalysis.ru

Pavel V. Snytnikov – Boreskov Institute of Catalysis, Lavrentiev Ave., 5, Novosibirsk, 630090, Russia; ORCID 0000-0002-5057-3187; pvsnyt@catalysis.ru

Anton V. Kuzmin – Department of Technology of Inorganic Materials and Electrochemical Production, Vyatka State University, Moskovskaya st., 36, Kirov, 610000, Russia; ORCID 0000-0002-0700-662X; a.v.kuzmin@yandex.ru

Conflict of interest: the authors declare no conflict of interest.